Features and Mechanism of H^- Anion Emission from $12CaO \cdot 7Al_2O_3$ Surface

Fan Huang,[†] Jiang Li,[†] Lian Wang,[†] Ting Dong,[†] Jing Tu,[†] Yoshifumi Torimoto,[‡] Masayoshi Sadakata,[‡] and Quanxin Li*,[†]

Department of Chemical Physics, Lab of Biomass Clean Energy, University of Science & Technology of China, Hefei, Anhui, 230026, P.R. China, and Department of Chemical System Engineering, School of Engineering, The University of Tokyo, 7−3−1 Hongo, Bunkyo-ku,Tokyo 113-8656, Japan

Received: January 3, 2005; In Final Form: May 1, 2005

The hydrogen anion (H^-) and other anionic species (O^-, OH^-, e^-) in the gas phase, emitted from the synthesized crystal surface of $12CaO \cdot 7Al_2O_3-H^-$ (C12A7−H^-), have been observed. The emission intensity of all the anionic species strongly depends on the sample surface temperature and the extraction field. H^- has the highest emission branch ratio, and the extraction field can reduce its apparent activation energy. H^- emission current at a $\mu A/cm^2$-level has been achieved, which is about 4 orders of magnitude higher than that obtained from the thermal desorption process of CaH_2. The observed anions of H^- and OH^- are attributed to their migration from the C12A7−H^- cages onto the surface [i.e., Y^-(cages) → Y^-(surface) → Y^-(gas phase) (Y = H, OH)]. The weak O^- and electron emission would both arise from the dissociation of O^{2-}: O^{2-}(surface) → O^-(surface) + e^-(surface) → O^-(gas phase) + e^-(space).

1. Introduction

Negative ions, most of which are key active chemical species, have wide potential applications in many fields, including chemistry, biomedicine, and material modifications.[1−6] For instance, as a typical anion, atomic oxygen radical anion (O^-) has an extremely high oxidation power and high reactivity, and it has been reported that O^- can react with methane on MgO even at 130 K.[7] The conventional method used to produce negative ions is the attachment of a free electron to a molecule or negative ion/molecule reactions, which could occur during electron impact, plasma, or laser irradiation processes.[1,8−9] However, the processes above are usually complicated, energetically costly, and generally accompanied by the formation of other ion species. Recently, we have developed a new way to obtain atomic oxygen radical anions O^- by using the Y_2O_3-stabilized ZrO_2 (YSZ),[10−12] which is simple and can easily be used in practical applications.

A hydrogen atom has one positively charged proton in the nucleus and one negatively charged electron orbiting the nucleus. The two opposite charges balance each other, resulting in no charge. Active hydrogen, known as H^-, on the other hand, contains two electrons orbiting the nucleus, creating a negative charge. H^- has engaged considerable attention in these years.[13−19] For instance, it has been reported that CaH_2 is concluded to be a good metal hydride for thermal desorption of H^- and could produce a not bad H^- emission current (about 10^{-10} A/cm^2).[18] On the other hand, there are many reports that show that H^- also plays an important role in the biomedicine field.[20−24] It has been found that massive energy generation (ATP production) is the fundamental core function of human cells and negatively charged electrons from hydrogen anions are the source of the energy needed to generate this staggering amount of ATP. Because of the essentiality of H^-, how to easily generate H^- becomes important. The common methods for producing H^- include hydrogen plasmas,[14] hydrogen dissociation on an oxide surface,[15] and the thermal desorption from metal hydride.[18] Recently, Flanagan and co-workers found that silica crystals dissolved in the water were able to hold H^-.[23] These compounds are technically called silica hydrides, and they have already applied silica hydrides to develop a new healthy medicine named MegaHydrin, which could supply enough H^- to the human body to serve as as an antioxidant.[20,24]

The compound $12CaO \cdot 7Al_2O_3$ (C12A7), one of the crystalline phases in the system of $CaCO_3$ and Al_2O_3, is a major constituent in aluminous cements, and in recent years, a number of studies have been reported on it.[25−38] The crystal structure of C12A7, containing two molecules per unit cell, is characterized by a positively charged lattice framework $[Ca_{24}Al_{28}O_{64}]^{4+}$ having 12 crystallographic cages per unit cell with a free space of ∼0.4 nm in diameter. The remaining two oxide ions (O^{2-}), referred to as "free oxygen", are clathrated in the cages to maintain charge neutrality.[25−26] With this special structure of C12A7, monocharge anions such as O^-, OH^- and halogen anions could substitute for free oxygen.[26−27] A particular characteristic of C12A7, encaging abundant O^- radicals and emitting a high density of O^- from its surface, recently has been reported.[32−33] The max O^- emission current achieved from this material (C12A7−O^-) is on the $\mu A/cm^2$ level, which is about 3 orders of magnitude higher than the current density emitted from the YSZ electrode surface. On the basis of these characteristics, Hayashi and co-workers successfully substituted H^- for O^- and formed the C12A7−H^- crystal.[39] In their works, they demonstrated an important property of C12A7−H^-: with light, C12A7−H^- can be converted into an electrical conductor, yielding electrical conductivity up to 0.3 $S \cdot cm^{-1}$. However, the emission property of this material remains unclear. In this contribution, we focused on the emission features and mechanism of C12A7−H^-. The emission behavior, including temperature and the extraction field effects, the emission branch ratio, and the emission current density have been studied.

* To whom correspondence should be addressed. E-mail: liqx@ustc.edu.cn.
[†] University of Science & Technology of China.
[‡] The University of Tokyo.

10.1021/jp050006g CCC: $30.25
Published on Web 06/01/2005

Furthermore, on the basis of these studies, the active energy of these anions emitting from the sample surface and the emission mechanism will be shown.

2. Experimental Section

The C12A7−O^- sample has been previously prepared:[33] Powders of $CaCO_3$ and γ-Al_2O_3 were mixed and grained at a molar ratio of $CaCO_3$:γ-Al_2O_3 = 12:7. The powder mixture was pressed in to a pellet with a diameter of 15 mm and a thickness of 1.5 mm. Then it was sintered at 1300 °C for 18 h and cooled to room temperature under flowing dry oxygen atmosphere. To obtain the C12A7−H^- sample, the initial C12A7−O^- sample was retreated at 1300 °C for 4 h in a hydrogen environment (10% H_2 buffered by 90% Ar) and then quenched to room temperature.

The experimental apparatus for studying the anionic emission has been described previously.[34] Briefly, it is made up of two major parts: a sample chamber and an ion-detection chamber with a time-of-flight (TOF) mass spectrometer, which was individually pumped by two turbo molecular pumps. The C12A7−H^- (or C12A7−O^-) sample was supported by a ship-like quartz tube, which was mounted in the center of the sampling chamber. The emission surface was opposite to the ion detector and heated radiatively by an Fe−Cr alloy filament. The heater was quartz-sealed in order to avoid the possible influence of electrons emitted from it upon our observations. The sample temperature was measured by a Ni/Cr thermocouple. The anions and electrons emitted from the surface were extracted by an extraction electrode, which is mounted opposite to the emission surface. The anionic collection electrode was connected to a picoammeter for emission current measurement. In the center of the collection plate, there was a 0.2 mm pinhole, which allowed simultaneous analysis for emitted species by TOF spectrometry. To make the measured distribution farthest near the real emission distributions, a calibration for our TOF mass spectrometer has been carried out before our experiments. Since the collection efficiencies of the emitted ions and electrons [defined by (detected particles cm^{-2}/emitted particles cm^{-2}) × η_{MCP}] depend on the length of the flight tube (l) and the MCP (microchannel plate) response efficiencies of the charge species (η_{MCP}), the detected ratio of a certain anion to the total anions, r, also depends on the length of the flight. To determine the r values on the sample emission surface, the l-dependence of r was approximately fitted to an exponential relation by measuring r as a function of the flight length (0.7−2.1 m). The present data of r were determined by an extrapolation value at $l = 0$ under fixed experimental conditions such as temperature and the extraction field. With the calibrated anionic distributions and the total emission currents, the emission current for a given species can be estimated. It should be pointed out that the anion emission intensity decreased upon increasing the emission time, particularly at higher temperature (>750 °C) and stronger extraction field (>500 V/cm). To guarantee an accurate measurement, the samples were changed when an obvious decrease of the emission intensity was observed, and a calibration was also performed in this work. On the other hand, the method to obtain a sustainable anion emission by continuously supplying H_2 and electrons can be realized, which will be described elsewhere. Before the C12A7−H^- sample was heated, the sample chamber was pumped to $<10^{-4}$ Pa so that the gas phase reaction was negligible. The leak current had been carefully checked; it was also negligible under our experimental conditions.

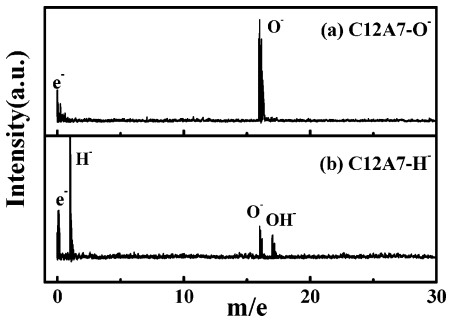

Figure 1. Typical TOF mass spectra for anions emitted from different sample surfaces at 750 °C and 800 V/cm: (a) C12A7−O^- sample and (b) C12A7−H^- sample.

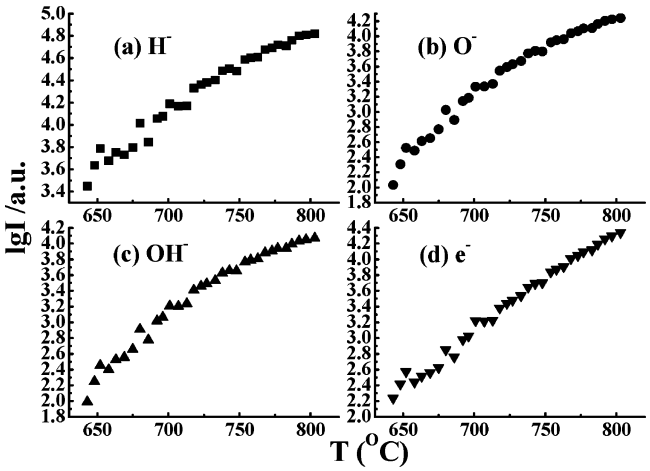

Figure 2. Temperature dependence of the anionic species at a given extraction field of 800 V/cm: (a) H^-, (b) O^-, (c) OH^-, and (d) e^-.

3. Results and Discussion

3.1. Emission Features of Anions and Electrons. The anion species emitted from the sample's front surface were identified by TOF mass spectrometry. For the initial C12A7−O^- sample, there are two peaks with the respective mass number of 16 and 0, which correspond to O^- and electrons, as shown in Figure 1a. The anionic species emitted from the C12A7−H^- sample are quite different from the C12A7−O^- sample, as shown in Figure 1b. Besides the peaks of O^- and electrons, two new peaks appear around the respective mass numbers of 1 and 17, which are attributed to the anions of H^- and OH^-. Meanwhile, the H^- peak is the strongest with other peaks all being weak.

The emission intensities of the anions and electrons from C12A7−H^- surface strongly depend on the sample temperature. We found that when the temperature was lower than 550 °C, the emission was so weak to be observed within our experimental sensitivity. As the temperature increased from 550 to 640 °C, the H^- peak appeared and became strong enough for measurement; however, the appearing frequency of O^- or OH^- was too low to make an accurate investigation. Only with the temperature higher than 640 °C could the emission intensities of all the anionic species be strong enough to make a quantitative analysis. Therefore, a temperature region from 640 to 800 °C was adopted in the present measurements. Figure 2 shows the typical temperature dependences of the emission intensities for H^-, O^-, OH^-, and electrons at a given extraction field of 800 V/cm.

Another significant characteristic for the C12A7−H^- sample is that the H^- emission is dominant, which is described by the emission branch ratio. The emission branch ratio of the anion

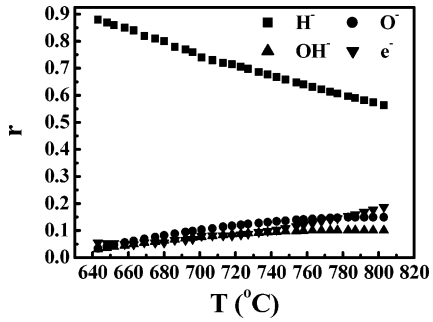

Figure 3. Emission branch ratios (r) of H^-, O^-, OH^-, and e^- as a function of surface temperature for the C12A7−H^- sample at a given extraction field of 800 V/cm.

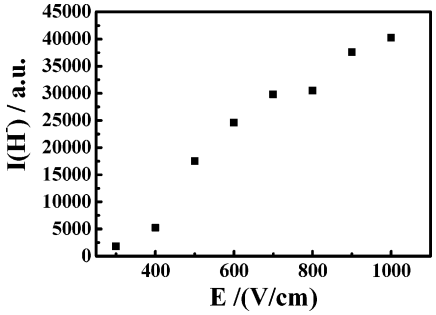

Figure 4. Emission intensities of H^- emitted from the C12A7−H^- sample surface as a function of the extraction field at 750 °C.

or electron, $r(X^-)$ (X = H, O, OH, or e), is defined as the relative intensity ratio of emitted anions or electrons of X^- to total anions and electrons, i.e., $r(H^-) = I(H^-)/[I(H^-) + I(O^-) + I(OH^-) + I(e^-)]$. Figure 3 shows the emission-branch ratios for H^-, O^-, OH^-, and electrons as a function of C12A7−H^- surface temperature at the extraction field of 800 V/cm. At the beginning temperature of ∼640 °C, the emission branch ratio of H^- reaches near 0.9, which is much stronger than that of O^-, OH^-, or e^- (all emission-branch ratios of them are near 0.05). When the temperature rises from ∼640 to 800 °C, $r(H^-)$ gradually decreases to ∼0.6, and $r(O^-)$ and $r(e^-)$, by contrast, both increase to ∼0.15. The emission-branch ratio of OH^- also increases from 0.03 at 640 °C to 0.1 at 800 °C with temperature rising, but not as much as O^- or e^-. The results showed above clearly demonstrate that H^- is the main anionic species emitted from the C12A7−H^- sample, and under certain conditions, a high purity of H^- emission could be obtained.

Furthermore, the emission intensity of H^- is also sensitive to the applied extraction field. Figure 4 displays a typical field dependence of the H^- emission at 750 °C. As the extraction field (E) less than 300 V/cm, the emission intensity of H^- is very weak, and no measurable emission was observed at $E = 0$ within our experimental detection limitation. When the extraction field is over 300 V/cm, the intensity of H^- remarkably increases an order of magnitude as the extraction field increases within our investigation region (300−1000 V/cm). The results above indicate that both the sample temperature and extraction field influence the H^- emission intensity.

To reveal further thermal and field effects on the H^- emission from C12A7−H^- sample, we replotted Figure 2a with a logarithm scale in the Arrhenius fashion (Figure 5), i.e., ln I versus $1/T$, implicitly testing the relation $I = A \exp(-E_a/RT)$, where A is the preexponential factor, R is the gas constant, and E_a is the apparent activation energy. Figure 5 exhibits a good Arrhenius relation with the apparent activation energy of 157.2 kJ/mol for H^- at an extraction field of 800 V/cm. Furthermore,

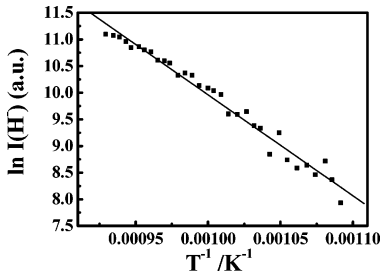

Figure 5. Arrhenius plot for emitted H^- from the C12A7−H^- sample surface at 800 V/cm.

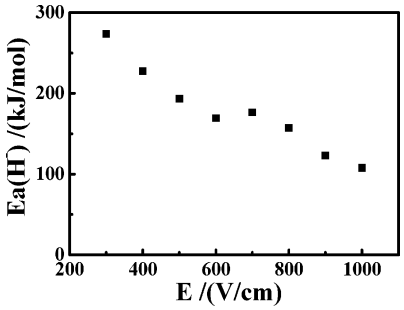

Figure 6. Apparent activation energies of H^- as a function of the extraction field.

TABLE 1: Activation Energies (E_a, kJ/mol) of H^-, O^-, OH^-, and e^- Measured at Different Extraction Fields

E/(V/cm)	H^-	O^-	OH^-	e^-
300	273.4	356.6	351.8	381.7
400	227.6	234.9	299.7	368.9
500	193.3	266.9	240.6	356.8
600	169.4	239.9	240.6	352
700	176.5	262.4	245.7	343
800	157.2	189.7	185.9	250.1
900	122.9	166.5	157.1	206.9
1000	107.6	150.1	152.2	214

we found that the activation energy of H^- is related to the applied extraction field, which is shown as Figure 6: with the extraction field rising from 300 to 1000 V/cm, the E_a of H^- drops down from 273.4 to 107.6 kJ/mol, which is at the same level as that of the O^- emitted from the C12A7−O^- sample.[34] For the apparent activation energies of O^-, OH^-, and electrons, they are similar to that of the H^-. Table 1 summarizes the apparent activation energies of all the anionic species obtained at different extraction fields.

3.2. H^- Emission Currents. Absolute emission current is one of the most important parameters for the anion emission materials, which was calculated from the relative intensity of TOF peaks and total emission current measured by the picoammeter. As mentioned in the Experimental Section, in the center of the collection plate, there was a 0.2 mm pinhole, which allowed us to simultaneously analyze the emitted anionic species by TOF spectrometry and measure absolute emission current. Total emission current density from C12A7−H^- can be expressed as follows:

$$I_t = I(H^-) + I(e^-) + I(OH^-) + I(O^-)$$
$$= \sum n_i q_i v_i \quad (i\text{: } H^-, e^-, O^-, \text{and } OH^-) \qquad (1)$$

where n_i, q_i, and v_i stand for the number density of the anions or electrons, the quantity of electric charge, and the speeds of ions or electrons, respectively. The speed of an ion or electron was estimated by measuring their flight time at a given flight

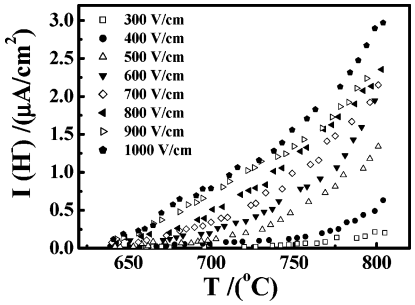

Figure 7. The absolute H^- emission current density versus the sample surface temperature at a series of extraction fields.

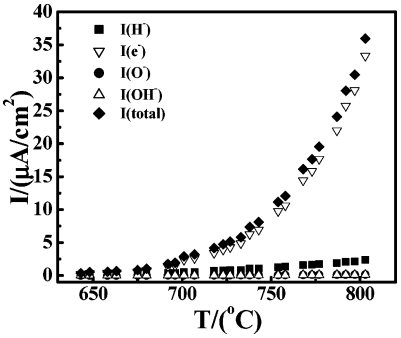

Figure 8. The emission current densities of e^-, H^-, O^-, and OH^- measured as a function of temperature at a given field of 800V/cm.

length. The relative ratio of the ion number density was approximately estimated by the emission branch ratio of different anions.

Figure 7 shows the H^- emission current densities measured at different extraction fields as a function of temperature. As forenamed, the emission current density shows temperature and field effects similar to those measured by TOF mass spectrometry. The maximum emission current density of H^- is 2.97 μA/cm^2 at 804 °C and 1000 V/cm in our investigated region, which is about 4 orders of magnitude higher than that of CaH_2.[18] Although there remains some problems such as the differences of the MCP sensitivity for the anions and electrons, which may cause the calculation of the current to be not accurate enough, we believe that the H^- anion is a dominant species emitted from the C12A7$-H^-$ sample and H^- emission current density can reach the μA/cm^2 level under our investigated conditions.

Figure 8 shows the estimated emission current densities of e^-, H^-, O^-, and OH^-, which were measured as a function of temperature at a given field of 800 V/cm. The emission current densities of e^-, H^-, O^-, and OH^- increased with increasing temperature. The ratio of the e^- current density to total emission current increased from 75% to about 90% as the temperature rises from 643 to 803 °C. Although H^- is the main species emitted from C12A7$-H^-$ (based on the emission branch ratio of H^-), the total emission current is still dominated by the e^- current density due to the speed of electron being much higher than that of H^-.

3.3. Emission Mechanism. $[Ca_{24}Al_{28}O_{64}]^{4+}{\cdot}2O^{2-}$ (C12A7) has a cubic structure with a lattice constant of 1.1989 nm. The most unique characteristics in the crystal structure are the positive charged lattice framework $[Ca_{24}Al_{28}O_{64}]^{4+}$ possessing 12 crystallographic cages per unit cell with a free space of 0.4 nm diameter. The remaining two oxide ions (O^{2-}), referred to as "free oxygen", exit in the cages.[25−26] It has been reported that a large amount of O^- can be formed and trapped in the cages of the C12A7 crystal, resulting in the formation of the C12A7$-O^-$ material.[32] The O^- emission from C12A7$-O^-$ has been proved: O^- anions in the cages migrate onto the sample surface by field-enhanced thermal diffusion and then are desorbed into the space to form the gas-phase anions [O^-(cages) → O^-(surface) → O^-(gas phase)].[34]

For the C12A7$-H^-$ sample, the H^- anion emission observed becomes dominant, although weak OH^- and O^- were also observed. These results would indicate that H^- and OH^- were formed and trapped in the cages of C12A7$-H^-$, leading to the substitution for O^- in the initial sinter process. It has also been demonstrated that the H^- anions exist in the cages of C12A7$-H^-$ by secondary ion mass spectroscopy (SIMS) and nuclear magnetic resonance (NMR) measurements.[39] The emission branch ratio of H^- is much larger than those of OH^- and O^-, which would imply that the concentration of the H^- anions in C12A7$-H^-$ is significantly higher than other anionic species such as OH^- and O^-. As mentioned above, the emission intensity of H^- increased upon increasing the sample temperature and the applied extraction field, because both temperature and field should enhance the migration rate and the desorption rate of the anions. Thus, similarly to the O^- emission from C12A7$-O^-$, we suggested that the H^- emission from C12A7$-H^-$ was formed by the following kinetic processes: the H^- anions in the cages migrated onto the sample surface by field-enhanced thermal diffusion and then are desorbed into the space to form the gas-phase anions, i.e., H^-(cages) → H^-(surface) → H^-(gas phase). In the same way, the OH^- anions observed would be formed through the reactions of O^- and/or O^{2-} with hydrogen in the high-temperature sinter process [O^-(cages) + H_2(gas-phase) → OH^-(cages) + H(gas-phase) and/or O^{2-}(cages) + H_2(gas-phase) → OH^-(cages) + H^-(cages)] and then desorbed into the space.

Meanwhile, our TOF measurements show that O^- and electron emission also appeared. It is well-known that a strong electrical field or high temperature may cause electron emission from a solid material surface.[40] Electron emission from a metal or semiconductor tip has been widely observed when a large electric field is applied between the tip and collection plate.[40−42] However, the electron emission from C12A7$-H^-$ sample could not be the field-induced electron emission, due to our applied field (usually smaller than 1000 V/cm) being too low to cause field-induced electron emission. As there should still be some free oxygen ions, O^{2-}, in the cages,[32] the possibility of O^- and e^- emission from C12A7$-H^-$ sample may both originate from the detachment process of O^{2-} occurring on the sample surface, which is explained for YSZ.[12] The emission process mentioned above can be expressed as O^{2-}(cages) → O^{2-}(frontside surface) → O^-(frontside surface) + e^-(frontside surface) → O^-(gas surface) + e^-(gas surface).

It was noted that the temperature dependence of the H^- emission measured by TOF-MS (time-of-flight mass spectroscopy) was quite different from that of H_2 desorption by TG−MS (thermogravimetric−mass spectroscopy). For the H^- emission from C12A7$-H^-$, we found that when the temperature was lower than 550 °C, the emission was too weak to be observed within our experimental sensitivity. As the temperature increased from 550 to 640 °C, the H^- peak appeared and became strong. The H^- emission remarkably increased with rising temperature from 640 to 800 °C. On the other hand, the temperature dependence of the H_2 desorption from C12A7$-H^-$ appeared with a broad profile, ranging from 500 to 750 °C with a center about 620 °C (see ref 39). We would like to emphasize that the above temperature behavior was well

reproduced, and similar characteristics of O^- and O_2 were also observed for the C12A7−O^- material (ref 34). For C12A7−O^-, the O^- emission increased with increasing temperature in the range of 500−820 °C (ref 34), but the O_2 desorption showed a broad profile in the range of 400−825 °C with a center about 740 °C (unpublished). The different temperature characteristics observed between the anion emission (H^- or O^-) and the neutral species' desorption (H_2 or O_2) may be attributed to different kinetic processes under different desorption conditions, as described below.

The H^- emission measurements were carried out under high vacuum condition ($<10^{-4}$ Pa). We attributed the observed H^- emission to H^-(cage) in the cages migrating to the surface (H^-(surface)) and then desorbing to the gas phase (H^-(gas phase)), which was presented as

$$H^-(\text{cage}) \rightarrow H^-(\text{surface}) \rightarrow H^-(\text{gas phase})\uparrow \quad (2)$$

Other species such as H_2^-(s) and H_2(s) may also form through the following surface reactions and desorbs into the gas phase:

$$H^-(\text{surface}) \rightarrow H(\text{surface}) + e^-(\text{surface})\uparrow \quad (3)$$

$$H(\text{surface}) + H^-(\text{surface}) \rightarrow H_2^-(\text{surface}) \rightarrow H_2^-(\text{gas phase})\uparrow \quad (4)$$

$$H(\text{surface}) + H(\text{surface}) \rightarrow H_2(\text{surface}) \rightarrow H_2(\text{gas phase})\uparrow \quad (5)$$

But we found that the desorption of H_2^- and H_2 from C12A7−H^- was neglectable under high vacuum conditions according to the investigation by TOF-MS and Q-MS (quadrupole mass spectroscopy). Thus, the H^- emission should be the dominant process under high vacuum conditions. Moreover, the emission intensity of H^- mainly depends on the concentration of H^-(cage) in the cages, the diffusion rate of H^-(cage) from the cage to the surface, and the desorption rate. The concentration of H^-(cage) decreases upon increasing the emission time, particularly at higher temperature (>750 °C). For example, it was found that the H^- emission intensity dropped to a half of the initial H^- intensity for more than 10 h at a fixed condition of 780 °C and an extraction field of 800 V/cm. To avoid the influence of concentration change on the investigation of the temperature effect, the samples were changed when an obvious decrease of the emission intensity was observed (less than 20%), and a calibration was also performed in this work (a method to obtain a sustainable anion emission by continuously supplying H_2 and electrons can be realized, which will be described elsewhere). Because both the anion's diffusion and desorption processes are enhanced by increasing temperature, it seems reasonable that the H^- emission intensity increases with increasing temperature.

On the other hand, the H_2 desorption from C12A7−H^- (ref 39) and O_2 desorption from C12A7−O^- (unpublished) have been observed by the TG−MS measurements under helium atmosphere conditions. The dependence of the H_2 and O_2 desportion on temperature appeared as broad profiles with the centers at 620 °C and 740 °C, respectively. The formation mechanism of H_2 and O_2 and their temperature characteristics remain unclear in the atmosphere. It was considered to be a complicated system, partly because many processes such as collision-induced energy transfer, surface reactions, and gas-phase reactions may occur, and partly because the anion's concentrations in the cages varied with the desorption time under those measurements. We suggest that the following processes could contribute the H_2 formation under the helium atmosphere condition:

$$H^-(\text{cage}) \rightarrow H^-(\text{surface}) \rightarrow H^-(\text{gas phase})\uparrow \quad (6)$$

$$H^-(\text{surface}) \text{ (by He collision)} \rightarrow H(\text{surface}) + e^-(\text{surface}) \rightarrow H(\text{gas phase})\uparrow \quad (7)$$

$$H(\text{surface}) + H^-(\text{surface}) \rightarrow H_2(\text{surface}) + e^-(\text{surface}) \rightarrow H_2(\text{gas phase})\uparrow \quad (8)$$

$$H(\text{surface}) + H(\text{surface}) \rightarrow H_2(\text{surface}) \rightarrow H_2(\text{gas phase})\uparrow \quad (9)$$

$$H(\text{gas phase}) + H(\text{gas phase}) \rightarrow H_2(\text{gas phase})\uparrow \quad (10)$$

Thus, the observed temperature behavior of H_2 may reflect an overall effect, such as the temperature effects of the H_2 (surface) formation and the H_2 (surface) desorption and the influence of the concentration change in the cages of C12A7−H^-. To make a clearer description for the temperature difference between the H^- emission and the H_2 desportion, particularly under atmospheric condition, we still need a lot of work to do.

4. Conclusions

We report a strong emission of the hydrogen anions (H^-) from the synthesized crystal of C12A7−H^- surface. The emission features of anions and electrons, including the temperature dependence, field characteristics, and emission branch ratios, have been investigated. H^- has the highest emission branch ratio, and a μA/cm^2 level H^- emission current has been achieved, which suggests that the C12A7−H^- sample can be used as a good H^- storage and emission material. The emission mechanisms of all the anionic species from the C12A7−H^- sample have been discussed. H^- and OH^- can migrate from the cages of the sample onto the front surface by the field-enhanced thermal diffusion and be desorbed into the space to form the anions of the gas phase. The weak O^- and electron emission, on the other hand, is supposed to arise from the dissociation of O^{2-} to a pair of O^- and e^-.

Acknowledgment. This research was supported by "BRP program" and "innovation program 2002" of Chinese Academy of Sciences. We thank Ms. Hui Xian, Mr. Chongfu Song, and Jianqiu Sun for the material synthesis.

References and Notes

(1) Ishikawa, J. *Rev. Sci. Instrum.* **1996**, *67*, 1410.
(2) Ishikawa, J. *Rev. Sci. Instrum.* **2000**, *71*, 1036.
(3) Tsuji, H.; Sato, H.; Baba, T.; Gotoh, Y.; Ishikawa, J. *Rev. Sci. Instrum.* 2**000**, *71*, 797.
(4) Lunsford, J. H. *Adv. Catal.* **1972**, *22*, 265.
(5) Che, M.; Tench, A. J. *Adv. Catal.* **1983**, *32*, 1.
(6) Valentine, J. S. *Active Oxygen in Biochemistry*; Blackie Academic & Professional: London, UK, 1995.
(7) Aika, K.; Lunsford, J. H. *J. Phys. Chem.* **1977**, *81*, 1393.
(8) Lee, J.; Grabowski, J. J. *Chem. Rev.* **1992**, *92*, 1611.
(9) Born, M.; Ingemann, S.; Nibbering, N. M. M. *Mass. Spectrom. Rev.* **1997**, *16*, 181.
(10) Torimoto, Y.; Harano, A.; Suda, T.; Sadakata, M. *Jpn. J. Appl. Phys.* **1997**, *36*, L238.
(11) Torimoto, Y.; Shimada, K.; Nishioka, M.; Sadakata, M. *J. Chem. Eng. Japan.* **2000**, *33*, 557.
(12) Nishioka, M.; Torimoto, Y.; Kashiwagi, H.; Li, Q.; Sadakata, M. *J. Catal.* **2003**, *215*, 1.
(13) Bressanini, D.; Morosi, G. *J. Chem. Phys.* **2003**, *119*, 14.
(14) Wang, W.; Xu, Y.; Wang, W.; Zhu, A. *J. Phys. D: Appl. Phys.* **2004**, *37*, 1185.

(15) Ito, T.; Sekino, T.; Moriai, N.; Tokuda, T. *J. Chem. Soc., Faraday Trans.* **1981**, *77*, 2181.
(16) Kawano, H.; Serizawa, N.; Takeda, M.; Maeda, T.; Tanaka, A.; Zhu, Y. *Thermochim. Acta* **1997**, *299*, 81.
(17) Steen, P. G.; Graham, W. G. *Appl. Phys. Lett.* **1999**, *75*, 18.
(18) Kawano, H.; Tanaka, A.; Sugimoto, S.; Iseki, T.; Zhu, Y.; Wada, M.; Sasao, M. *Rev. Sci. Instrum.* **2000**, *71*, 2.
(19) Parenteau, L.; Jay-Gerin, J. P.; Sanche, L. *J. Phys. Chem.* **1994**, *98*, 10277.
(20) Stephanson, C. J.; Stephanson, A. M.; Flanagan, G. P. *J. Med. Food.* **2002**, *5*, 9.
(21) Stephanson, C. J.; Stephanson, A. M.; Flanagan, G. P. *J. Med. Food.* **2003**, *6*, 249.
(22) Stephanson, C. J.; Flanagan, G. P. *Free Radic. Biol. Med*. **2003**, *35*, 1129.
(23) Stephanson, C. J.; Flanagan, G. P. *Int. J. Hydrogen Energy* **2003**, *28*, 1243.
(24) Stephanson, C. J.; Flanagan, G. P. *Int. J. Hydrogen Energy* **2004**, *29*, 459.
(25) Bartl, H.; Scheller, T. *Neues Jahrb. Mineral. Monatsh*. **1970**, *35*, 547.
(26) Jeevaratnam, J.; Glasser, F. P.; Glasser, L. S. D. *J. Am. Ceram. Soc*. **1964**, *47*, 105.
(27) Imlach, J. A.; Glasser, L. S. D.; Glasser, F. P. *Cem. Concr. Res*. **1971**, *1*, 57.
(28) Sung, Y. M.; Dunn, S. A.; Koutsky, J. A. *Ceram. Int*. **1995**, *21*, 169.
(29) Li, W.; Mitchell, B. S. *J. Non-Cryst. Solids* **1999**, *255*, 199.
(30) Mitchell, B. S. *Mater. Lett*. **2001**, *48*, 316.
(31) Watauchi, S.; Tanaka, I.; Hayashi, K.; Hirano, M.; Hosono, H. *J. Cryst. Growth* **2002**, *237*, 801.
(32) Hayashi, K.; Hirano, M.; Matsuishi, S.; Hosono, H. *J. Am. Chem. Soc*. **2002**, *124*, 738.
(33) Li, Q. X.; Hayashi, K.; Nishioka, M.; Kashiwagi, H.; Hirano, M.; Torimoto, Y.; Hosono, H.; Sadakata, M. *Appl. Phys. Lett*. **2002**, *80*, 4259.
(34) Li, Q. X.; Hosono, H.; Hirano, M.; Hayashi, K.; Nishioka, M.; Kashiwagi, H.; Torimoto, Y.; Sadakata, M. *Surf. Sci*. **2003**, *527*, 100.
(35) Hayashi, K.; Matsuishi, S.; Ueda, N.; Hirano, M.; Hosono, H. *Chem. Mater*. **2003**, *15*, 1851.
(36) Zhang, J.; Zhang, Z.; Wang, T.; Hao, W. *Mater. Lett*. **2003**, *57*, 4315.
(37) Matsuishi, S.; Toda, Y.; Miyakawa, M.; Hayashi, K.; Kamiya, T.; Hirano, M.; Tanaka, I.; Hosono, H. *Science* **2003**, *301*, 626.
(38) Toda, Y.; Matsuishi, S.; Hayashi, K.; Ueda, K.; Kamiya, T.; Hirano, M.; Hosono, H. *Adv. Mater*. **2004**, *16*, 685.
(39) Hayashi, K.; Matsuishi, S.; Kamiya, T.; Hirano, M.; Hosono, H. *Nature* **2002**, *419*, 462.
(40) Somorjai, G. A. *Introduction to Surface Chemistry and Catalysis;* John Wiley and Sons: New York, 1994, p 381.
(41) Zhu, W.; Kochanski, G. P.; Jin, S. *Science* **1998**, *282*, 1471.
(42) Geis, M. W.; Efremow, N. N.; Krohn, K. E.; Twichell, J. C.; Lyszczarz, T. M.; Kalish, R.; Greer, J. A.; Tabat, M. D. *Nature* **1998**, *393*, 431.